Journal of Translational Medicine

RESEARCH

Open Access

BMP9 enhances osteogenic differentiation in rheumatoid arthritis: a potential therapeutic approach

Han Zhang[1†], Zixian Dang[1†], Xiangyu Wang[1†], Changyao Wang[1], Haining Zhang[1] and Yongtao Zhang[1*]

Abstract

Objective Rheumatoid arthritis (RA) is a chronic inflammatory disorder that causes joint damage, including cartilage degradation and bone erosion. Bone morphogenetic protein 9 (BMP9), a member of the TGF-β superfamily, plays a key role in osteogenesis and tissue repair. However, its role in bone erosion and inflammation in RA remains underexplored. This study aims to evaluate BMP9's therapeutic potential in RA, focusing on its effects on bone destruction, osteogenesis, and inflammation.

Materials and methods In this study, BMP9 expression was analyzed in synovial tissues from RA and osteoarthritis patients and in the ankle joints of collagen-induced arthritis (CIA) mice using immunohistochemistry, qRT-PCR, and Western blotting. The therapeutic effect of BMP9 on bone destruction was evaluated in a CIA mouse model through micro-CT imaging, histological analysis, and clinical scoring. Osteogenic differentiation was assessed by alkaline phosphatase and Alizarin Red S staining, while osteoclast activity was examined through tartrate-resistant acid phosphatase staining. Fluorescence double-labeling was used to track new bone formation. Data were analyzed using (Statistical Package for the Social Sciences) SPSS, and appropriate statistical tests were performed to determine significance.

Results In this study, BMP9 expression was significantly down-regulated in the synovial tissue of RA patients and in the ankle joints of CIA mice. BMP9 treatment in CIA mice ameliorated joint inflammation, as shown by reduced limb swelling, lower arthritis index, and improved tissue morphology. Furthermore, BMP9 significantly alleviated bone loss, as evidenced by increased bone mineral density and trabecular structure. However, BMP9 treatment did not significantly impact osteoclastogenesis or bone resorption. BMP9 also enhanced bone mineralization and formation, as shown by increased mineral apposition rate and bone formation rate. Additionally, BMP9 promoted osteogenic differentiation of synovial cells, enhancing alkaline phosphatase activity and mineral nodule formation. These results suggest that BMP9 has a protective effect on joint inflammation and bone loss in RA, potentially through promoting bone formation without influencing osteoclast activity.

Conclusion Our study concludes that targeting BMP9 alleviates inflammation and promotes osteogenic differentiation in RA, highlighting BMP9 as a promising therapeutic target for addressing bone destruction in RA.

Keywords BMP9, Rheumatoid arthritis, Osteogenic differentiation, Bone destruction, Inflammation

[†]Han Zhang, Zixian Dang, and Xiangyu Wang have contributed equally to this work and share first authorship.

*Correspondence:
Yongtao Zhang
drzhang215@163.com

Introduction

Rheumatoid arthritis (RA) is a common chronic inflammatory joint disease that primarily affects the joints, often leading to cartilage and bone damage, as well as disability. It is also a systemic syndrome with extra-articular manifestations, including rheumatoid nodules, pulmonary involvement, vasculitis, and systemic comorbidities [1, 2]. RA significantly impairs physical function and quality of life, placing a substantial burden on individuals and society. The global incidence of RA ranges from 0.5 to 1%, with regional variations [3–5]. Bone erosion and systemic bone loss in RA arise from an imbalance in the osteoblast-osteoclast axis, which disrupts bone homeostasis. This imbalance is characterized by excessive bone resorption mediated by osteoclasts and impaired bone formation due to osteoblast dysfunction. It plays a central role in RA pathogenesis, leading to joint erosion. If untreated, it can result in extensive bone loss, joint destruction, and irreversible damage, ultimately causing pain, deformity, and disability, further decreasing the quality of life for RA patients [6–8]. Therefore, developing therapeutic strategies that restore bone homeostasis and promote osteoblast activity is essential for improving the prognosis of RA.

Bone morphogenetic proteins (BMPs), also known as growth differentiation factor 2, are members of the transforming growth factor-beta (TGF-β) superfamily and play a crucial role in bone formation and stem cell differentiation [9–11]. Bone morphogenetic protein 9(BMP9) is primarily produced in the liver and circulates in the bloodstream as a pleiotropic cytokine that regulates the proliferation and differentiation of various cell types. Its receptors include ALK1 and ALK2, and it exhibits multiple pharmacological effects, such as antifibrotic, antitumor, anti-heart failure, and antidiabetic activities [12, 13]. Although the role of BMP9 in promoting osteoblast differentiation, enhancing bone formation, and improving fracture healing in estrogen deficiency-induced osteoporosis is well established [13–15], its potential therapeutic applications in RA remain underexplored. Recent studies suggest that BMP9 can stimulate osteogenesis, making it a promising candidate for treating RA-associated bone erosion [14, 16–19]. Given its osteogenic properties, BMP9 offers a unique therapeutic opportunity to promote osteogenesis in RA, addressing one of the most challenging aspects of disease management. In addition to its effects on bone formation, BMP9 also has anti-inflammatory properties, showing potential in controlling inflammation associated with various tissue diseases, such as vascular diseases, liver fibrosis, osteoarthritis (OA), and cancer. Treatment with BMP9 has been shown to significantly alter the levels of inflammatory factors (IL-6, IL-8, and TNF-α), chemokines, and inflammatory signaling pathways in hepatic stellate cells and endothelial cells, potentially providing additional benefits for RA patients [20–23]. Recent evidence indicates that the BMP signaling pathway is activated in the synovium of RA patients and in collagen-induced arthritis (CIA) models [24, 25]. Furthermore, both BMP2 and TGF-β1 have been shown to inhibit the expression of the pro-inflammatory cytokine IL-34 in RA synovial fibroblasts [26]. Additionally, studies have found that BMP9 inhibits the proliferation and migration of RA fibroblast-like synoviocytes by modulating the PI3K/AKT signaling pathway [27]. Despite these promising findings, the molecular mechanisms by which BMP9 mediates bone remodeling and its effects on the immune system in the context of RA remain poorly understood. Investigating how BMP9 interacts with these pathways, particularly in osteoblasts, is critical for the development of targeted therapies for RA.

In this study, we aim to explore the potential of BMP9 to promote osteogenesis and reduce arthritis-related inflammation in RA. Given that RA is characterized by excessive bone resorption and chronic inflammation, BMP9's dual ability to stimulate osteoblast differentiation and modulate inflammatory responses offers a promising therapeutic approach. Furthermore, we will assess its potential as a novel treatment for RA, ultimately providing new insights into the management of the disease.

Materials and methods

Patient samples and tissue collection

A total of 6 patients were included in the study, comprising 3 RA patients (2 females, 1 male, aged 61–75 years) and 3 OA patients (3 females, aged 63–79 years). Synovial tissue samples were obtained during total knee arthroplasty from all participants. The collected samples were used in three independent experiments, as described below. One portion of each sample was fixed in 4% paraformaldehyde, embedded in paraffin, and sectioned into 4 μm slices for immunohistochemical staining. The remaining tissue was stored at −80 °C for Western blot and real-time polymerase chain reaction (RT-PCR) analysis. This study was approved by the Ethics Committee of Qingdao University Affiliated Hospital, and all participants provided written informed consent to participate.

Animal model and BMP9 treatment

Forty healthy 8-week-old male DBA/1J mice were randomly allocated into four groups (n = 10/group):.Sham operation (SHAM)/Control (CONT), CIA, CIA + BMP9, CIA + Green Fluorescent Protein (GFP). The CIA model was established following established protocols [28]. Firstly, chicken type II collagen stock solution (2 mg/mL, Sigma, USA) was emulsified in complete Freund's

adjuvant at a 1:1 ratio to prepare the primary emulsion (1.5 mg/mL). Then, each mouse received 0.1 mL of this emulsion through multi-site intradermal tail injections. Finally, on day 21 post-primary immunization, a secondary emulsion was prepared by emulsifying type II collagen with incomplete Freund's adjuvant (Sigma, USA) at 1:1 ratio. Mice received 0.1 mL booster injections using the same delivery method.

Mice in the SHAM/Control group were subjected to the same injection procedure as the CIA group, but with saline solution instead of chicken type II collagen and Freund's adjuvant. This group served as a baseline control to evaluate the effects of the injection procedure and viral vector administration without inducing arthritis.

For BMP9 treatment, recombinant BMP9 adenovirus (1×10^8 (Plaque Forming Unit) PFU) was injected into the right knee joints of the CIA mice at weeks 0, 2, 4, and 6. Fluorescence imaging was performed at weeks 1, 3, 5, and 7 to track the local concentration of BMP9 following the initial BMP9 adenovirus injection.

Mice in the CIA + GFP group underwent the same procedure as the CIA group to induce arthritis. Following arthritis induction, these mice were administered a GFP adenoviral vector, which served as a viral vector control. The GFP gene within the adenovirus co-expressed as a tracking marker, enabling the monitoring of infected cells and the assessment of viral distribution through fluorescence microscopy. This allowed for the observation of the delivery and localization of the GFP adenovirus in joint tissues, providing a control to evaluate the effects of the viral vector in the absence of therapeutic BMP9 treatment. The animal experiments were approved by the relevant Ethics Committee.

Hematoxylin and eosin (H&E) staining method

Mouse ankle tissue sections and synovial tissue sections from RA and OA patients were stained with H&E and subsequently examined and photographed under a microscope. H&E staining was performed to assess the histopathological changes in the tissue samples. The morphological features were evaluated as histological score by two pathologists in a blinded manner. Briefly, after paraffin embedding, tissue sections were cut into 4 μm thick slices. These sections were deparaffinized by immersion in xylene, followed by rehydration through a graded ethanol series (100, 95, and 70%). The sections were then stained with Hematoxylin for 5–10 min to stain the cell nuclei, followed by rinsing in running tap water to remove excess stain. Next, the sections were stained with eosin for 2–5 min to stain the cytoplasm and extracellular matrix. After staining, the sections were dehydrated in a graded ethanol series (70, 95, and 100%), cleared in xylene, and mounted with a coverslip using neutral balsam. Finally, the stained slides were analyzed under a light microscope for histological evaluation.

Immunohistochemistry

Immunohistochemical staining of BMP9 was performed on the mouse ankle tissue sections and the synovial tissue sections of OA or RA patients. After a standard deparaffinization procedure, the sections were incubated with 0.3% hydrogen peroxidase for 15 min at room temperature, followed by antigen retrieval using 0.01 M citrate buffer at 80 °C for 20 min. Subsequently, the sections were blocked with normal goat serum for 30 min at room temperature, incubated with primary antibodies against BMP9(1:200, Abcam Cat# ab128874, RRID:AB_11145462), and then incubated with biotinylated secondary antibody (Zhongshan Golabrige Biotechnology, China) followed by horseradish peroxidase-conjugated streptavidin (Zhongshan Golabrige Biotechnology, China). The ultimate reaction product was visualized with diaminobenzidine. The stained signals were captured and photographed by the Leica Microsystems (Wetzlar, Germany). The experiment was performed in triplicate.

Clinical arthritis scoring of mice

Arthritis Severity Scoring in the mice was assessed using the following scale:0 Normal paw.

0: Normal paw.

1: One toe inflamed and swollen.

2: More than one toe inflamed and swollen, but not the entire paw; or mild swelling of the entire paw.

3: Entire paw inflamed and swollen.

4: Very inflamed and swollen paw, or ankylosed paw. If the paw is ankylosed, the mouse is unable to grip the wire top of the cage.

The total score was obtained by calculating the sum of the four paws of a mouse. The scores were recorded every seven days after the second injection until one day before sacrifice.

Micro-computed tomography (CT) imaging and bone histomorphometric analysis

This experiment employed three-dimensional CT reconstruction to analyze various bone morphometric parameters, including bone mineral density (BMD), bone volume to tissue volume ratio (BV/TV), bone surface to bone volume ratio (BS/BV), and trabecular number (Tb.N). Tartrate-resistant acid phosphatase (TRAP) staining was conducted on mouse ankle tissue sections using a commercial TRAP kit sourced from Nanjing Jiancheng Biotechnology Company, China. Microscopic analysis was performed to assess the degree of bone resorption, and the following metrics were obtained: the

number of TRAP-positive multinucleated osteoclasts per bone surface (N.OC/BS), the ratio of osteoclast surface to bone surface (OCs/BS), and the ratio of eroded surface to bone surface (ES/BS). All experiments were conducted in triplicate. The equipment utilized in this study was the SCANCO μCT100, which is designed for high-resolution micro-CT analysis.

Fluorescence calcein and Alizarin red staining (ARS)

The ankle tissues of mice, embedded in undecalcified methyl methacrylate, were sectioned into 5 μm slices and examined using a fluorescence microscope (EEVOS FL, Invitrogen by Thermo Fisher Scientific, Germany). Calcein/ARS labeling was recorded to evaluate bone formation by measuring various bone mass parameters, including the bone formation rate (BFR) per bone surface (BFR/BS), mineral adherence rate (MAR), and the ratio of mineralized surface to bone surface (MS/BS). The experiment was conducted in triplicate.

Western blot

Tissue samples were lysed on ice using Radioimmunoprecipitation Assay (RIPA) buffer (Solarbio, China) containing 1% protease inhibitor (Solarbio, China). The lysates were then centrifuged at 10,000×*g* for 10 min at 4 °C, and the supernatants were collected for analysis. Protein concentrations were determined using the BCA protein assay kit (Solarbio, China). The protein samples were mixed with loading buffer and heated at 95 °C for 5 min. Equal amounts of protein were then loaded onto 10% SDS-PAGE gels, and electrophoresis was performed for 120 min at 90 V. Following this, proteins were transferred onto PVDF membranes at 290 mA for 90 min. The membranes were blocked for 1.5 h with 5% fat-free milk in Tris-buffered saline-Tween(TBST), followed by overnight incubation at 4 °C with primary antibodies (BMP9, Abcam, UK, 1:1000; GAPDH, Cell Signaling Technology, USA, 1:2000). After three TBST washes, the membranes were incubated with HRP-conjugated secondary antibodies (Cell Signaling Technology, USA, 1:5000). Target bands were detected using ECL PLUS reagent (Sigma, USA) and imaged with a BioSpectrum Imaging System (UVP, Thermo Fisher Scientific, USA). Quantification of results was carried out using Image J software and normalized to GAPDH levels. The experiment was performed in triplicate.

RT-PCR

Total RNA was isolated from tissues using TRIzol reagent (TaKaRa, Japan) under RNase-free conditions. RNA concentration and purity were assessed using an ultraviolet spectrophotometer (Implant, Munich, Germany). Next, RNA was reverse transcribed into complementary DNA (cDNA) using the Revert Aid First Strand cDNA Synthesis kit (TaKaRa, Japan). The cDNA was diluted and used as templates for PCR. mRNA levels of the target genes were measured using the SYBR Green PCR master mix (TaKaRa, Japan), with all PCR reactions conducted in triplicate. RT-PCR was carried out on a LightCycler® 96 system (Roche, Indianapolis, IN, USA) under the following conditions: 95 °C for 10 min; followed by 40 cycles of 95 °C for 10 s, 60 °C for 10 s, and 72 °C for 15 s. Relative gene expression was normalized to GAPDH and analyzed using the $2^{-\Delta\Delta Ct}$ method. Primer sequences were designed using Primer 3 Plus and are listed in Table 1. The experiment was performed in triplicate.

BMP9 adenovirus construction and transfection

To construct the BMP9 recombinant adenovirus, the AdEasy system was employed [29]. Initially, the coding region of the human BMP9 gene was amplified using Hi-Fi PCR and subsequently cloned into the adenoviral shuttle vector. The recombinant adenoviral vector was then transfected into packaging cells (e.g., 293pTP cells) to generate the BMP9-containing recombinant adenovirus (Ad-BMP9). Additionally, the vector co-expressed GFP as a tracking marker, enabling the monitoring of infected cells via fluorescence microscopy. The transfected 293pTP cells were cultured at 37 °C in 5% CO_2. Once typical adenovirus infection symptoms, such as cell fusion and lysis, were observed, the culture supernatant was collected, and viral particles were purified by centrifugation. Through ultracentrifugation, the viral particles were separated and resuspended in an appropriate buffer to obtain a high-concentration viral solution. The viral titer was estimated by evaluating the percentage of GFP-positive cells using fluorescence microscopy.

To enhance adenovirus infection efficiency, 5 μg/ml of Polybrene was added during all infection steps. Target cells, such as mouse bone marrow stromal cells (imBMSCs), were seeded in 24-well plates and infected when they reached 60–80% confluence. During infection, the

Table 1 Primer sequences for RT-PCR

Target gene	Primer sequences (5′–3′)
BMP9 (Human)	F: GGAAGGAAACATGGTCGTTTAC
	R: CATCCTGAATGTCCTGGGATAC
GAPDH (Human)	F: CTCTGACTTCAACAGCGACAC
	R: TACCAGGAAATGAGCTTGACAA
BMP9 (Mouse)	F: CAGAACTGGGAACAAGCATCC
	R: GCCGCTGAGGTTAAGGCTG
GAPDH (Mouse)	F: ATGGGTGTGAACCACGAGA
	R: CAGGGATGATGTTCTGGGCA

Ad-BMP9 viral solution was co-cultured with the cells for 24 h, after which the medium was replaced with fresh culture medium. Post-transfection, GFP was used as a marker to monitor the transfection efficiency under a fluorescence microscope. After infection, the effects of BMP9 expression were observed, and the role of BMP9 in bone formation was further assessed. The present study evaluated the local concentration changes of BMP9 in the knee joint through multiple injections of BMP9 adenovirus. The present study evaluated the local concentration changes of BMP9 in the knee joint through multiple injections of BMP9 adenovirus. The experimental procedure was as follows: BMP9 adenovirus was injected into knee joints at week 0, 2, 4, and 6, followed by virus imaging one week later. All the experiments were performed in triplicate.

Cell culture

Synovial cells used in this study were isolated from patients with RA who underwent knee joint replacement surgery. All patients met the diagnostic criteria for RA as defined by the American College of Rheumatology revised classification criteria [30]. Informed consent was obtained from each patient, and the study protocol was approved by the Ethics Committee of the Affiliated Hospital of Qingdao University. During surgery, synovial tissue was harvested, minced, and digested with Type I collagenase (Sigma, USA) in DMEM supplemented with 1% penicillin and streptomycin (Gibco BRL, USA) and 10% fetal bovine serum (Gibco BRL, USA) at 37 °C. Cells were cultured and passaged, and synovial cells from passages 3 to 8 were used for subsequent experiments. Cells from each patient were used independently in different experiments to ensure the independence of each experimental group.

ARS

After 21 days of osteogenic induction, the cells were washed with PBS and fixed in 2.5% glutaraldehyde for 15 min. Following another PBS wash, the cells were stained with alizarin red (Sigma, USA) at room temperature for 20 min. Images were captured using a microscope, and calcium nodules were identified as red spots. The alizarin red staining was quantitatively analyzed according to a previous method [31]. Briefly, the alizarin red stain was extracted using 10% acetic acid (Sigma, USA), neutralized with 10% ammonium hydroxide (Sigma, USA), and the optical density was measured at 405 nm.

Alkaline phosphatase (ALP) staining

After three and five days of osteogenic induction, the cells were fixed in 4% paraformaldehyde for 15 min and subsequently incubated with ALP (Solarbio, China) at 37 °C in the dark for 20 min. Images were then obtained using a microscope. This experiment was repeated three times.

Statistical analysis

Statistical analyses were performed using SPSS 26.0 (SPSS Inc., Chicago, IL, USA). Data are expressed as the mean ± standard deviation (SD). Differences among groups were analyzed using Kruskal–Wallis test, one-way analysis of variance test, or Student's t-test. A value of $p < 0.05$ was considered statistically significant for all analyses.

Results

BMP9 expression is down-regulated in RA synovium compared to OA

The following results demonstrated that BMP9 expression was down-regulated in the synovial tissue of RA patients. Immunohistochemical analysis revealed that BMP9 expression in the synovium of RA patients was significantly lower than that in OA patients (Fig. 1A). WB analysis showed a significant decrease in the relative ratio of BMP9 to GAPDH protein in RA patients ($^{*}p < 0.05$, $^{**}p < 0.01$, Fig. 1B, C). Additionally, lower levels of BMP9 mRNA were detected in the RA synovium (Fig. 1D). Taken together, these results suggested that BMP9 was down-regulated in the synovial tissue of RA patients.

BMP9 expression was down-regulated in the ankle joints of CIA mice

The immunohistochemistry results showed that BMP9 was expressed in mouse ankle tissues from control group and CIA group, and the expression in the CIA group was lower than that in the control group (Fig. 2A). In addition, the CIA group presented significantly decreased BMP9 expression at protein level (Fig. 2B, C) and the mRNA level (Fig. 2D) as compared with the control group. These results demonstrated that BMP9 was down-regulated in the ankle tissues of mice with arthritis induced by collagen.

Establishment of the CIA mouse model and the down-regulation of BMP9 expression in the knee joint

The present study evaluated the local concentration changes of BMP9 in the knee joint through multiple injections of BMP9 adenovirus. The experimental procedure was as follows: BMP9 adenovirus was injected into both knee joints at week 0, followed by virus imaging one week later. The results showed high fluorescence intensity in both knee joints. Subsequently, BMP9 adenovirus injections were administered only to the right knee joint

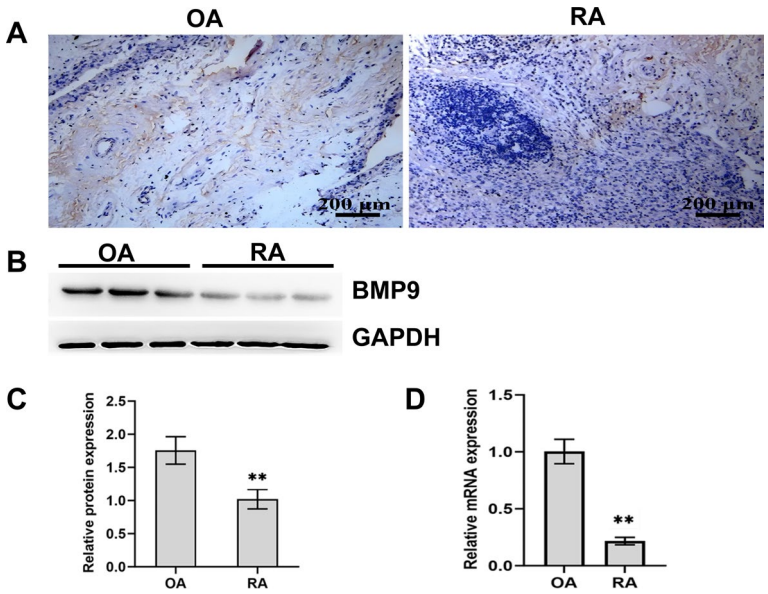

Fig. 1 Down-regulated BMP9 expression in the knee synovial tissue from patients with RA. The levels of BMP9 in the synovial tissue from patients with either OA or RA were determined by immunohistochemistry, Western blot, and RT-PCR. Data are representative images or expressed as the mean ± SD of each group from three separate experiments (n = 3 per group). **A** Representative images of immunohistochemistry (magnification ×100) show more inflammatory hyperplasia in RA synovial tissue, with a lower expression of BMP9 compared to OA. **B**, **C** Western blot. **D** RT-PCR. *$p < 0.05$ vs. the OA group. **$p < 0.01$ vs. the OA group

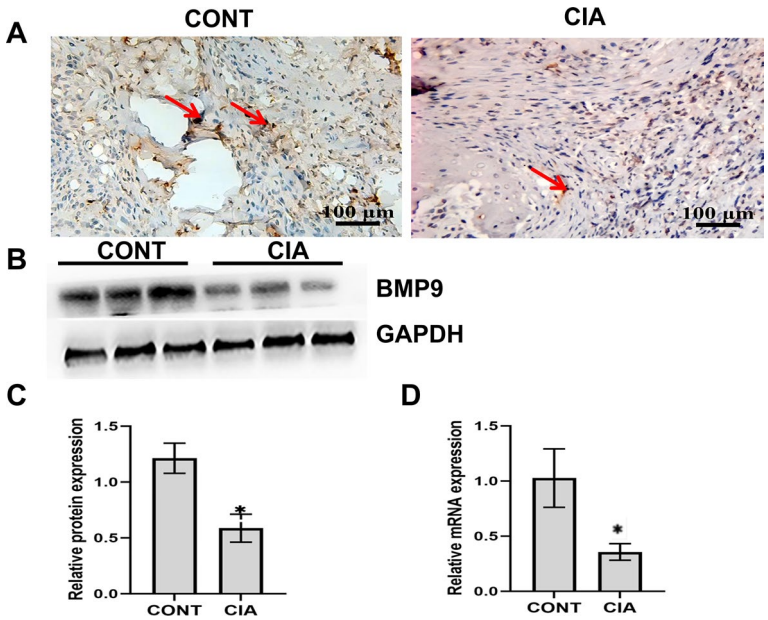

Fig. 2 Down-regulated BMP9 expression in the ankle tissues of CIA mice. The levels of BMP9 in the ankle tissues of collagen-induced arthritis (CIA) mice were determined by immunohistochemistry, Western blot, and RT-PCR. Data are representative images or expressed as the mean ± SD of each group from three separate experiments (n = 3 per group). **A** Representative immunohistochemistry images (magnification ×200). **B**, **C** Western blot. **D** RT-PCR. *$p < 0.05$ vs. the control group; **$p < 0.01$ vs. the control group

at weeks 2, 4, and 6, while the left knee joint remained untreated, and imaging analysis was performed one week after each injection. The results indicated that BMP9 concentration remained high in the right knee joint after each injection, whereas the concentration in the left knee joint gradually decreased. Ultimately, regular BMP9

adenovirus injections successfully maintained a high BMP9 concentration in the right knee joint (Fig. 3A). This experimental protocol will be applied to all subsequent experiments.

Immunohistochemical analysis (Fig. 3B) showed higher BMP9 expression in the SHAM group, a significant reduction in BMP9 expression in the CIA group, a marked increase in BMP9 expression in the CIA + BMP9 group, and BMP9 expression in the CIA + GFP group that was similar to the CIA group. Western blot analysis (Figs. 3C, D) further quantified the BMP9 protein expression levels. The SHAM group showed the normal baseline BMP9 concentration. Compared to the SHAM group, BMP9 expression was significantly lower in the CIA group ($^{**}p < 0.01$). In the CIA + BMP9 group, BMP9 expression was significantly higher than in both the CIA and CIA + GFP groups. BMP9 expression in the CIA + GFP group was significantly lower compared to the CIA + BMP9 group, with statistical significance ($^{\#\#}p < 0.01$).

BMP9 ameliorated joint inflammation and injury in CIA mice

Compared to the control mice, the CIA mice exhibited significantly higher limb swelling. However, in the CIA + BMP9 group, ankle joint swelling was notably reduced compared to both the CIA and CIA + GFP groups (Fig. 4A). H&E staining revealed extensive inflammatory cell infiltration in the CIA mice, with synovial tissue invading the joint space, loss of normal ankle joint morphology, and more pronounced focal bone erosion. In contrast, BMP9 treatment resulted in a significant reduction in inflammatory cell numbers and a marked improvement in tissue morphology (Fig. 4B). The arthritis index in the CIA + BMP9 group was significantly lower than that in both the CIA and CIA + GFP groups ($p < 0.05$), indicating that BMP9 has anti-inflammatory effects (Fig. 4C). Histological scoring of arthritis severity showed that the CIA + BMP9 group had significantly lower scores compared to both

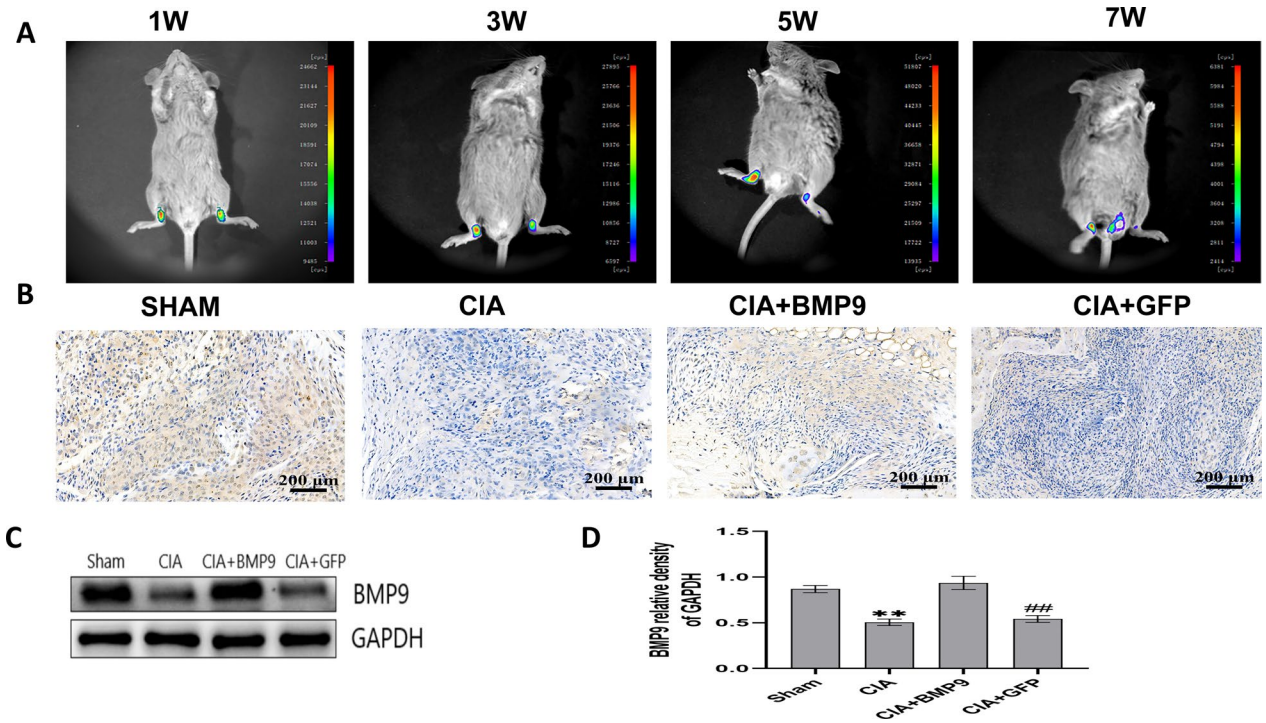

Fig. 3 Establishment of the CIA mouse model and the down-regulation of BMP9 expression in the knee joint. **A** Fluorescence imaging results showed that, after BMP9 adenovirus injection, the fluorescence signal in the right knee joint remained consistently high at 1, 3, 5, and 7 weeks, while the fluorescence signal in the left knee joint, which did not receive subsequent BMP9 injections, gradually diminished. This suggests that BMP9 can maintain a high local concentration after injection, but the concentration in the untreated area significantly decreased over time. **B** Immunohistochemical analysis showed higher BMP9 expression in the SHAM group, a significant reduction in BMP9 expression in the CIA group, a marked increase in BMP9 expression in the CIA + BMP9 group, and BMP9 expression in the CIA + GFP group that was similar to that in the CIA group. **C**, **D** Western blot analysis further quantified the BMP9 protein expression levels in each group. The SHAM group displayed the normal baseline BMP9 concentration. Compared to the SHAM group, BMP9 expression was significantly lower in the CIA group ($^{**}p < 0.01$). In the CIA + BMP9 group, BMP9 expression was significantly higher than in both the CIA and CIA + GFP groups. The BMP9 expression in the CIA + GFP group was significantly lower compared to the CIA + BMP9 group, with statistical significance ($^{\#\#}p < 0.01$)

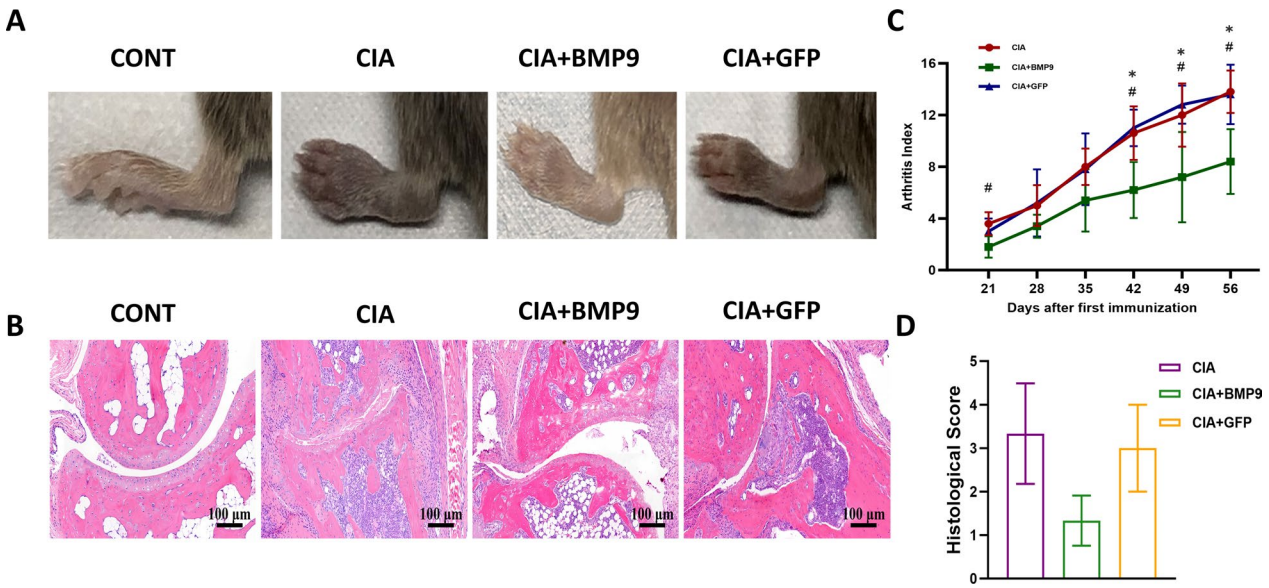

Fig. 4 BMP9 ameliorated joint inflammation and injury in CIA mice. **A** In the CIA + BMP9 group, ankle joint swelling was significantly reduced compared to both the CIA and CIA + GFP groups. **B** H&E staining revealed that, in the CIA + BMP9 group, the number of inflammatory cells was markedly reduced, and histological morphology showed significant improvement compared to the CIA and CIA + GFP groups. **C** Arthritis index scores showed that the CIA + BMP9 group had a significantly lower arthritis index than both the CIA and CIA + GFP groups ($p < 0.05$), indicating that BMP9 has a significant anti-inflammatory effect. **D** Histological scoring of arthritis severity showed that the CIA + BMP9 group had significantly lower scores compared to both the CIA and CIA + GFP groups ($p < 0.05$), further confirming the therapeutic efficacy of BMP9 in alleviating arthritis

the CIA and CIA + GFP groups ($p < 0.05$, Fig. 4D), which was consistent with the clinical arthritis scores.

BMP9 alleviated bone loss in CIA mice

The bone quality and related quantitative metrics of mice from different treatment groups, as assessed by Micro-CT. Figure 5A shows significant bone loss and severe trabecular destruction in the CIA group, while BMP9 treatment (CIA + BMP9 group) partially restored bone quality, with relatively intact trabecular structure. Quantitative analysis revealed that BMP9 significantly increased BMD,Tb.N, and showed statistical differences compared to the CIA group ($^*p < 0.05$). Additionally, while there were no significant differences ($p > 0.05$), BMP9 treatment led to an increase in the bone volume-to-tissue volume ratio (BV/TV) and bone surface-to-bone volume ratio (BS/BV) compared to the CIA group (Fig. 5B–E). These results suggest that BMP9 has a significant protective and restorative effect on bone loss in the CIA model.

BMP9 treatment did not significantly impact osteoclastogenesis or bone resorption

In the CIA model, BMP9 treatment did not significantly impact osteoclastogenesis or bone resorption. TRAP staining revealed a significant increase in osteoclast numbers in the CIA group, but BMP9 treatment did not notably affect osteoclast quantity. Quantitative analysis showed that the number of osteoclasts (Oc.N), bone resorption surface (ES/BS), and osteoclast surface area (OC.S/BS) were not significantly different between the BMP9 group and the CIA or CIA + GFP groups ($p > 0.05$). These results suggest that BMP9 did not exert a significant effect on osteoclast formation or bone resorption in this model (Fig. 6).

Effect of BMP9 on bone mineralization and formation in the CIA model.

Double-labeling fluorescence analysis revealed significantly reduced new bone deposition in the CIA group, with sparse green and red markings, indicating impaired mineralization dynamics. In contrast, the BMP9 treatment group showed significantly increased new bone deposition, with dense fluorescence labeling approaching control group levels. Quantitative analysis further demonstrated that the MAR in the BMP9 group was significantly higher than in the CIA group ($^*p < 0.05$) and was similar to that of the control group. The bone formation rate (BFR/BS) was significantly higher in the BMP9 group compared to both the CIA and CIA + GFP groups ($^{**}p < 0.01$), nearly reaching normal levels. Additionally, the percentage of MS/BS was significantly increased in the BMP9 group compared to the CIA + GFP group ($^*p < 0.05$). These results indicate that BMP9 treatment

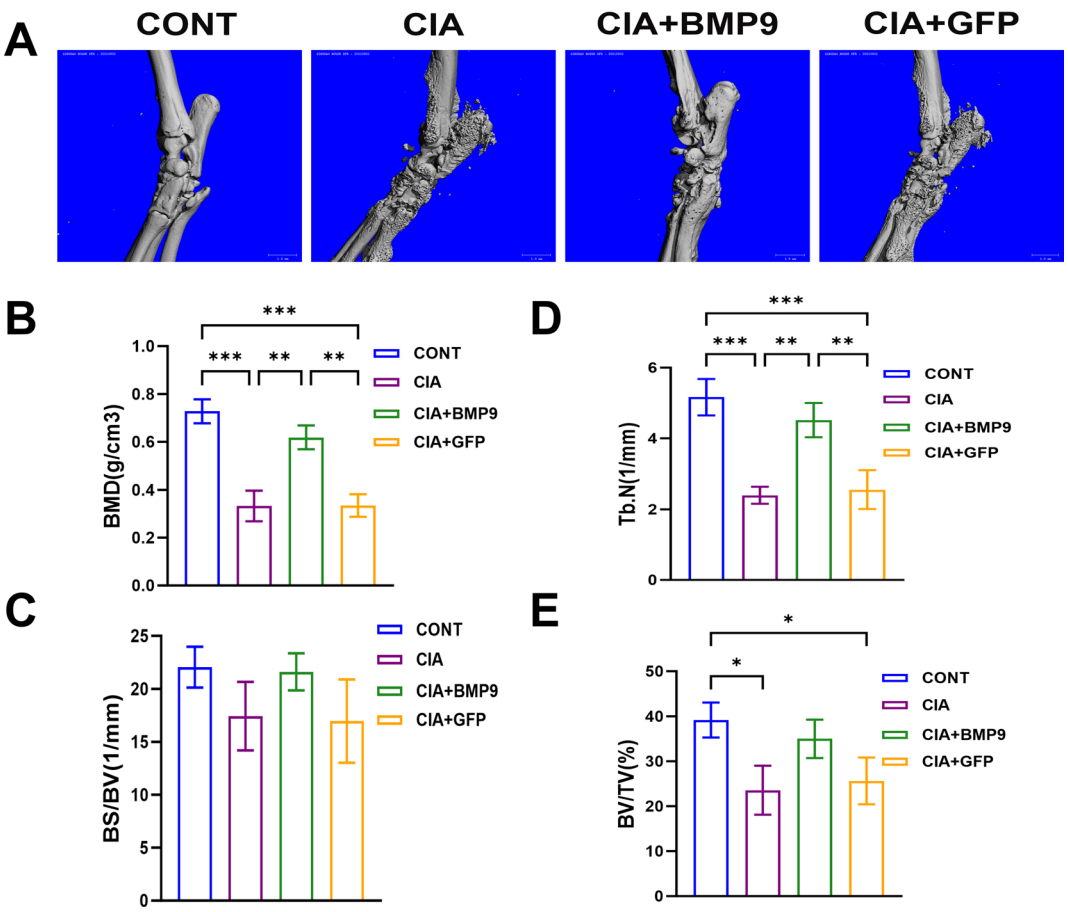

Fig. 5 The bone quality and related quantitative metrics of mice from different treatment groups, as assessed by Micro-CT. **A** shows significant bone loss and severe trabecular destruction in the CIA group, while BMP9 treatment (CIA + BMP9 group) partially restored bone quality, with relatively intact trabecular structure. Quantitative analysis revealed that BMP9 significantly increased bone mineral density (BMD), trabecular number (Tb.N), and showed statistical differences compared to the CIA group (*$p < 0.05$). Additionally, while there were no significant differences ($p > 0.05$), BMP9 treatment led to an increase in the bone volume-to-tissue volume ratio (BV/TV) and bone surface-to-bone volume ratio (BS/BV) compared to the CIA group (**B**–**E**). These results suggest that BMP9 has a significant protective and restorative effect on bone loss in the collagen-induced arthritis model

significantly enhances bone mineralization and formation in the CIA model (Fig. 7).

BMP9 enhances osteogenic differentiation of synovial cells by promoting ALP activity and mineral nodule formation

In this study, BMP9 transfection was successfully achieved, as indicated by the bright green fluorescence observed in the BMP9 group (Fig. 8A). BMP9 treatment significantly enhanced ALP activity, with ALP expression levels significantly higher in the BMP9 group compared to the control and GFP groups at both day 3 and day 5 (Fig. 8B, C, G; *$p < 0.05$). Additionally, BMP9 treatment promoted mineral nodule formation, with ARS staining at 7 and 14 days revealing more extensive and darker mineralization in the BMP9 group (Fig. 8D, E). Quantitative analysis of ARS absorbance demonstrated significantly higher mineralization levels in the BMP9 group at both time points compared to the control and GFP groups (*$p < 0.05$, Fig. 8F). These results demonstrate that BMP9 significantly enhances the osteogenic differentiation of synovial cells, as evidenced by increased ALP activity and enhanced mineralization.

Discussion

This study provides a comprehensive examination of the role of BMP9 in RA, focusing on its potential to promote osteogenic differentiation. Our initial findings revealed a significant downregulation of BMP9 expression in the synovial tissue of RA patients, which was notably lower than in OA patients. This was further confirmed through immunohistochemistry, Western blotting, and RT-PCR analyses, suggesting that BMP9 plays a crucial regulatory role in the pathogenesis of RA. Through experiments using a CIA mouse model, we observed that BMP9

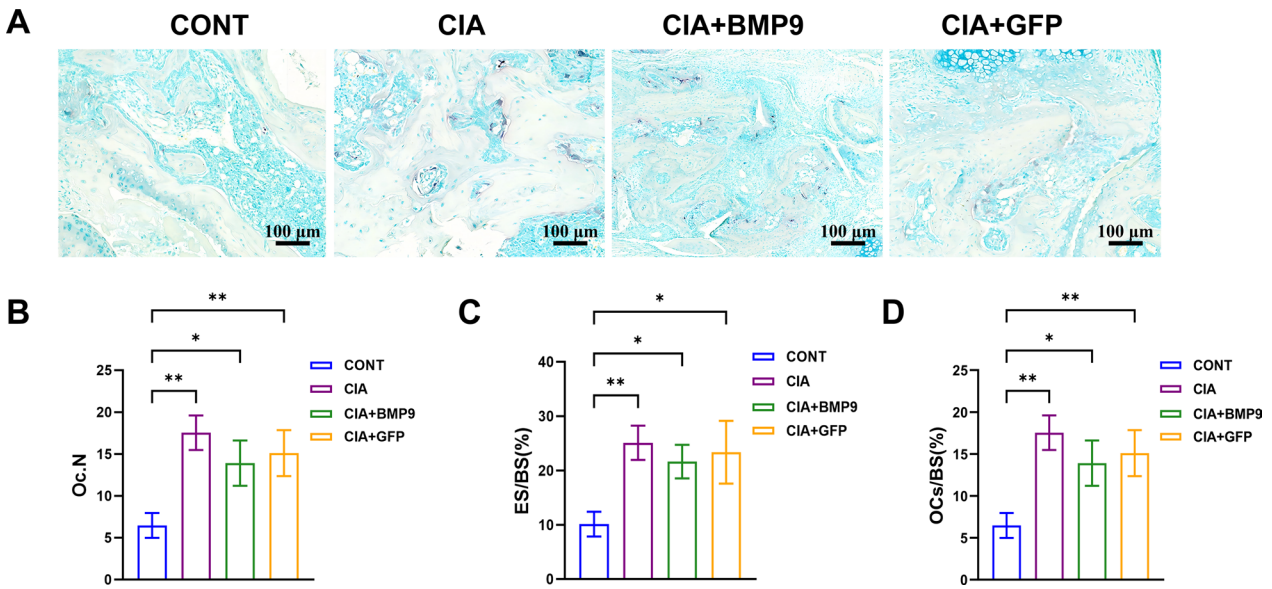

Fig. 6 BMP9 treatment did not significantly impact osteoclastogenesis or bone resorption. **A** TRAP staining results are shown for different experimental groups. TRAP staining is primarily used to label osteoclasts. The results indicated a significant increase in osteoclast number in the CIA group, while BMP9 treatment did not significantly affect osteoclast numbers. **B** The number of osteoclasts (Oc.N) in each group is shown. In the BMP9 group, the osteoclast count was not significantly different from the CIA or CIA + GFP groups ($p > 0.05$), suggesting that BMP9 did not significantly influence osteoclast formation or quantity. **C** Measurement of bone resorption surface (ES/BS) is shown. There was no significant difference in the ES/BS between the BMP9 group and the CIA or CIA + GFP groups ($p > 0.05$), indicating that BMP9 did not significantly improve bone resorption. **D** Measurement of osteoclast surface area (OC.s/BS) is shown. The osteoclast surface area in the BMP9 group did not differ significantly from that in the CIA or CIA + GFP groups ($p > 0.05$), further supporting that BMP9 did not significantly affect osteoclast formation

deficiency exacerbated joint inflammation, while BMP9 supplementation significantly improved the pathological condition of RA mice. BMP9 treatment not only suppressed joint inflammation but also promoted osteoblast differentiation and the formation of mineralized nodules, enhancing trabecular bone repair and regeneration. Furthermore, we found that BMP9 upregulated osteogenic markers, such as increased ALP staining expression, and facilitated mineralized nodule formation, further supporting its potential in bone repair and regeneration. These results are consistent with previous studies that have shown BMP9 promotes osteogenic differentiation and activates the Wnt/β-catenin signaling pathway by upregulating LGR6, while inhibiting osteoclastogenesis through suppression of Akt1 phosphorylation [14]. This leads to improved bone mass, microstructure, and strength, as well as reduced bone resorption [14]. Additionally, research has demonstrated that BMP9-induced bone marrow mesenchymal stem cells (BMSCs) exhibit effective osteogenic differentiation both in vitro and in vivo, highlighting BMP9 as a promising candidate for bone defect repair [32]. In comparative studies of BMPs using adenoviral transfection, BMP9 has shown superior osteogenic potential compared to the clinically approved BMP-2 and BMP-7 [33]. Moreover, BMP9 has been shown to upregulate DLX6-AS1, which promotes odontogenic/osteogenic differentiation of dental pulp cells through the miR-128-3p/MAPK14 axis [34]. Other studies have reported that LGR4 enhances BMP9-induced osteogenesis, where BMP9 upregulates LGR4 expression via the mTORC1/Stat3 pathway, leading to enhanced osteoblast differentiation and inhibition of adipogenesis [35]. In contrast, the study found that Lox modulates BMP9-induced osteogenesis by inhibiting HIF-1α expression, thus suppressing the Wnt/β-catenin signaling pathway and reducing BMP9's osteogenic potential [21]. Interestingly, our research also shows that BMP9 treatment significantly improved bone density in RA mice. These findings are consistent with existing literature, which highlights the osteogenic role of BMP9 in various bone disease animal models, suggesting that BMP9 induction could serve as a potential therapeutic approach for conditions such as osteoporosis, fractures, and bone defects [14, 15]. These results highlight BMP9 as a key osteogenic factor, suggesting that BMP9 may promote bone repair by stimulating local osteogenic responses, making it a promising therapeutic target for bone metabolic diseases such as RA.

Additionally, our study demonstrates that BMP9 treatment not only promotes osteogenesis but also improves arthritis inflammation in mice. This is consistent with previous research, which highlights BMP9 as a unique

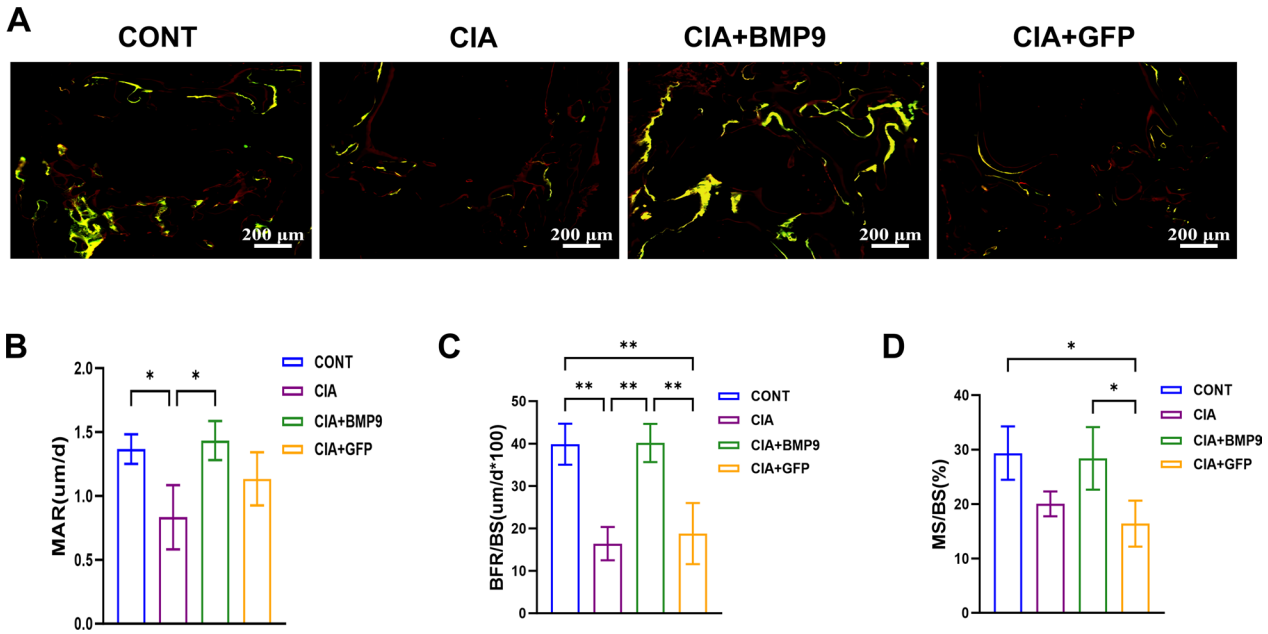

Fig. 7 Effect of BMP9 on bone mineralization and formation in the CIA model. (1) Double-labeling fluorescence results (**A**): Fluorescence labeling showed that new bone deposition was significantly reduced in the CIA group, with sparse green and red markings, indicating impaired mineralization dynamics. In contrast, the BMP9-treated group exhibited significantly increased new bone deposition compared to the CIA and CIA + GFP groups, with dense fluorescence labeling, approaching the levels observed in the control group. (2) Quantitative analysis (**B**–**D**): Mineral apposition rate (MAR) (**B**): The mineralization apposition rate in the BMP9 group was significantly higher than that in the CIA group (*$p < 0.05$), and was similar to the normal control group. Bone formation rate (BFR/BS) (**C**): The BMP9-treated group showed a significantly higher BFR/BS than both the CIA and CIA + GFP groups (**$p < 0.01$), almost reaching normal levels.Mineralized surface percentage (MS/BS) (**D**): The BMP9-treated group showed a significant increase in the percentage of the mineralized surface, with a significant difference compared to the CIA + GFP group (*$p < 0.05$)

member of the BMP family that is increasingly recognized for its role in regulating inflammation and it emphasize its complex involvement in tissue inflammation and its potential as a key mediator of inflammatory responses [36]. Interestingly, another study using the dystrophin-/-/utrophin-/- double knockout (dKO-Hom) mouse model found that the downregulation of BMP9 and inflammatory factors such as IL-4 during tibial fracture healing was associated with muscle damage, leading to impaired osteoclast and osteoblast generation and significantly delaying fracture healing [37]. In RA, fibroblast-like synoviocytes (FLS) actively promote inflammation through the production of pro-inflammatory cytokines and mediators, such as TNF-α and IL-6 [38]. A recent study further showed that after 24 days, BMP9 expression in a rat arthritis model was reduced, and BMP9 knockdown and overexpression promoted and inhibited FLS proliferation and migration, respectively [27]. BMP9 may regulate FLS in atherosclerosis, and its downregulation in arthritis synovial tissue, likely due to different inflammatory environments, is crucial for inflammation progression, while its overexpression promotes cartilage repair in OA mice [39]. Another study confirmed that BMP2 and BMP9 can partially block the inhibition of chondrogenic differentiation in MSCs by low IL-1β concentrations; however, BMP9 can maintain high expression of Col2A1 regardless of IL-1β levels [40, 41]. Additionally, one study showed that LPS inhibited BMP9-induced osteogenic differentiation in vitro, affecting BMP9 through the MAPK pathway [42]. Another study also suggests that BMP9 may act as a cytokine to counteract bone lesions caused by chronic inflammation, presenting a key and promising perspective. TNF-α was found to attenuate BMP9-induced osteogenic differentiation in human periodontal ligament fibroblasts and rat dental follicle cells [23, 43]. These findings indicate that BMP9 may exert a critical role in promoting osteogenesis through these inflammatory mechanisms.

Despite the promising results observed in our mouse models, there are several limitations in this study that should be addressed in future research. One key limitation is the lack of an in-depth exploration of the underlying mechanisms through which BMP9 influences RA. To address this, future studies will focus on uncovering the molecular pathways through which BMP9 mediates its effects on joint inflammation and bone loss in RA. Another limitation concerns the recombinant adenovirus used to express BMP9, which lacks inherent tissue

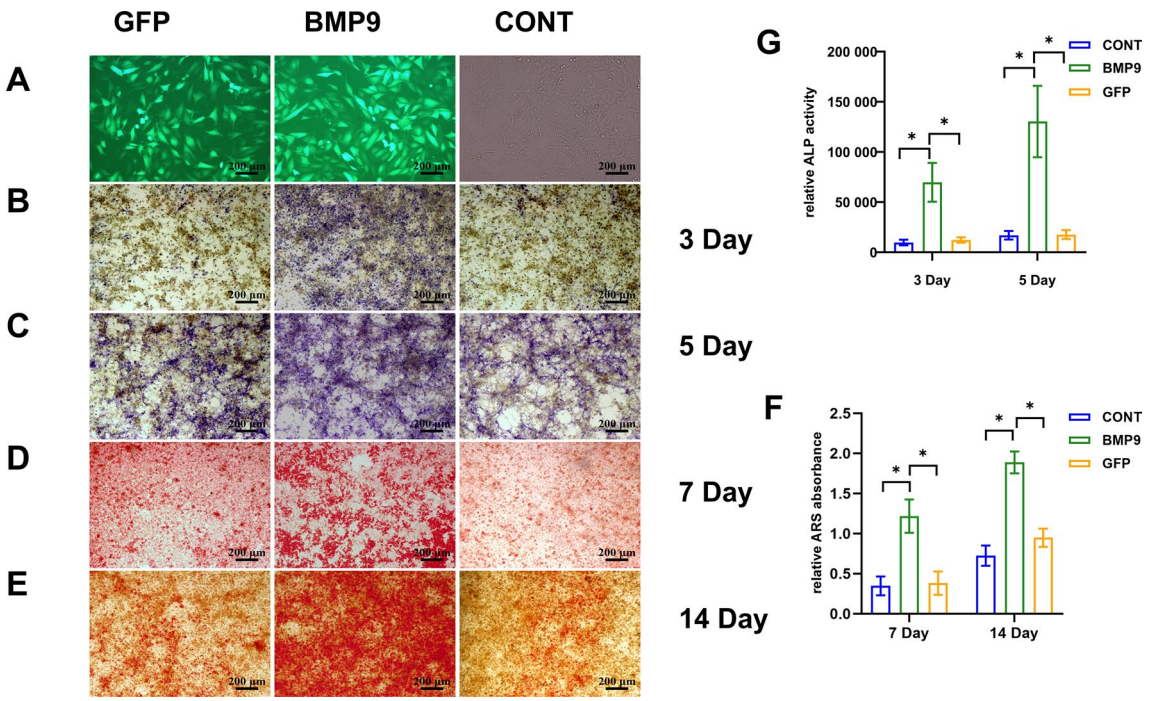

Fig. 8 BMP9 enhances osteogenic differentiation of synovial cells by promoting ALP activity and the formation of mineralized nodules. (1) Successful BMP9 Transfection (**A**): BMP9 expression was observed under a fluorescence microscope. Cells in the BMP9 group exhibited bright green fluorescence, indicating successful and efficient transfection. (2) BMP9 Significantly Promotes ALP Activity (**B**, **C**, **G**): ALP staining at 3 and 5 days showed that the BMP9-treated group had significantly higher ALP expression compared to the control and GFP groups. Quantitative analysis revealed that ALP activity was significantly increased in the BMP9 group on both day 3 and day 5, with statistical significance (*$p < 0.05$). (3) BMP9 Promotes Mineral Nodule Formation: ARS staining at 7 and 14 days showed that the BMP9 group exhibited a more widespread distribution of mineralized nodules with a darker color, indicating significantly enhanced mineralization (**D**, **E**). ARS absorbance measurements showed that the BMP9 group had significantly higher mineralization levels at both day 7 and day 14 compared to the control and GFP groups, with statistical significance (*$p < 0.05$, **F**)

specificity. Although we ensured targeted delivery to the ankle joint via local injections, the adenovirus can still infect a broad range of cells [44]. Moving forward, we plan to explore more tissue-specific delivery methods to improve the precision of BMP9 targeting and reduce potential off-target effects. Finally, while this study primarily focused on the therapeutic effects of BMP9 via overexpression, future research will involve incorporating synovium-specific BMP9 knockdown or knockout models. This will help clarify the precise role of BMP9 in RA pathogenesis and enable a more comprehensive understanding of its therapeutic potential.

Conclusion

Our study underscores BMP9's innovative therapeutic potential in RA, showing its ability to promote osteoblast differentiation and target inflammation—two key pathological features of RA. BMP9 offers a promising approach to combat RA-related bone loss, a challenge current therapies cannot fully address. While BMP9 shows significant efficacy in preclinical mouse models, further research is needed to clarify its mechanisms, optimize delivery, and validate its safety and effectiveness in clinical trials, offering a potential new treatment strategy for RA.

Abbreviations

RA	Rheumatoid arthritis
qRT-PCR	Quantitative real-time PCR
CIA	Collagen-induced arthritis
TNF-α	Tumor necrosis factor α
IL-1	Interleukin-1
IL-6	Interleukin-6
FLS	Fibroblast-like synoviocytes
OA	Osteoarthritis
BMPs	Bone morphogenetic proteins
BMP9	Bone morphogenetic protein 9
GFP	Green fluorescent protein
CT	Computed tomography (CT)
Ad-BMP9	BMP9-containing recombinant adenovirus
H&E	Hematoxylin and eosin
CONT	Control
TRAP	Tartrate-resistant acid phosphatase
BMD	Bone mineral density
BV	Bone volume to ratio
TV	Tissue volume
Tb.N	Trabecular number
OCs	Osteoclast surface
ES	Eroded surface
BS	Bone surface
BFR	Bone formation rate

PFU	Plaque forming unit
MAR	Mineral adherence rate
MS	Mineralized surface
BS	Bone surface
cDNA	Complementary DNA
ALP	Alkaline phosphatase
RIPA	Radioimmunoprecipitation assay
BCA	Bicinchoninic acid
SD	Standard deviation
TBST	Tris-buffered saline-Tween

Supplementary Information

The online version contains supplementary material available at https://doi.org/10.1186/s12967-025-06309-5.

Additional file 1.

Additional file 2.

Acknowledgements
We would like to express our sincere gratitude to the Young Elite Sponsorship Program of Shandong Provincial Medical Association for providing financial support for this study (grant number 2023_LC_0267). We also thank the Qingdao Outstanding Health Professional Development Fund for their support (grant number 4355)

Author contributions
Study Design: WCY, ZYT. Data Collection: WXY, ZH. Statistical Analysis: ZH, WXY. Data Interpretation: WXY, ZH, DZX, WCY. Manuscript Preparation: WXY, DZX, ZYT, ZH. Literature Search: WXY, ZHN, ZH. Funds Collection: ZYT. ZH and ZYT wrote the main manuscript text. ZH, ZYT, WXY, WCY and ZHN prepared Figures 1–8. All authors reviewed the manuscript.

Funding
Funding for this study was provided by Young Elite Sponsorship Program of Shandong Provincial Medical Association [grant number 2023_LC_0267] and Supported by Qingdao Outstanding Health Professional Development Fund [grant number 4355].

Availability of data and materials
The datasets used in the current study are available from the corresponding author on request.

Declarations

Ethics approval and consent to participate
All participants in this study gave informed consent prior to their inclusion. The animal experiments were conducted in accordance with the National Research Council's Guide for the Care and Use of Laboratory Animals. The study protocols were approved by the Ethical Committee of the Affiliated Hospital of Qingdao University and the Animal Experimentation Ethics Committee of Qingdao University.

Consent for publication
All authors gave their consent for publication and have no conflicts of interest.

Competing interests
The authors declare that they have no competing interests.

Author details
[1]Department of Orthopedics, The Affiliated Hospital of Qingdao University, Qingdao 266000, Shandong, China.

Received: 3 January 2025 Accepted: 23 February 2025
Published online: 28 February 2025

References

1. Smolen JS, Aletaha D, McInnes IB. Rheumatoid arthritis. Lancet. 2016;388(10055):2023–38.
2. Gravallese EM, et al. What Is rheumatoid arthritis? N Engl J Med. 2024;390(13): e32.
3. Cross M, et al. The global burden of rheumatoid arthritis: estimates from the global burden of disease 2010 study. Ann Rheum Dis. 2014;73(7):1316–22.
4. Silman AJ, Pearson JE. Epidemiology and genetics of rheumatoid arthritis. Arthritis Res. 2002;4 Suppl 3(Suppl 3):S265–72.
5. Alamanos Y, Voulgari PV, Drosos AA. Incidence and prevalence of rheumatoid arthritis, based on the 1987 American College of Rheumatology criteria: a systematic review. Semin Arthritis Rheum. 2006;36(3):182–8.
6. O'Neil LJ, Kaplan MJ. Neutrophils in rheumatoid arthritis: breaking immune tolerance and fueling disease. Trends Mol Med. 2019;25(3):215–27.
7. Maruotti N, Corrado A, Cantatore FP. Osteoporosis and rheumatic diseases. Reumatismo. 2014;66(2):125–35.
8. Bellavia D, et al. Vitamin D level between calcium-phosphorus homeostasis and immune system: new perspective in osteoporosis. Curr Osteoporos Rep. 2024;22(6):599–610.
9. Wang RN, et al. Bone Morphogenetic Protein (BMP) signaling in development and human diseases. Genes Dis. 2014;1(1):87–105.
10. Lamplot JD, et al. BMP9 signaling in stem cell differentiation and osteogenesis. Am J Stem Cells. 2013;2(1):1–21.
11. Whitton A, et al. Differential spatial regulation of BMP molecules is associated with single-suture craniosynostosis. J Neurosurg Pediatr. 2016;18(1):83–91.
12. Bouvard C, et al. Different cardiovascular and pulmonary phenotypes for single- and double-knock-out mice deficient in BMP9 and BMP10. Cardiovasc Res. 2022;118(7):1805–20.
13. Chen X, et al. Emodin promotes the osteogenesis of MC3T3-E1 cells via BMP-9/Smad pathway and exerts a preventive effect in ovariectomized rats. Acta Biochim Biophys Sin (Shanghai). 2017;49(10):867–78.
14. Zhou Y, et al. BMP9 reduces bone loss in ovariectomized mice by dual regulation of bone remodeling. J Bone Miner Res. 2020;35(5):978–93.
15. Wang X, et al. Bone morphogenetic protein 9 stimulates callus formation in osteoporotic rats during fracture healing. Mol Med Rep. 2017;15(5):2537–45.
16. Yao H, et al. TGFbeta1 induces bone formation from BMP9-activated bone mesenchymal stem cells, with possible involvement of non-canonical pathways. Int J Med Sci. 2020;17(12):1692–703.
17. Siverino C, et al. Addition of heparin binding sites strongly increases the bone forming capabilities of BMP9 in vivo. Bioact Mater. 2023;29:241–50.
18. Zhang J, et al. Lysyl oxidase inhibits BMP9-induced osteoblastic differentiation through reducing Wnt/beta-catenin via HIF-1a repression in 3T3-L1 cells. J Orthop Surg Res. 2023;18(1):911.
19. Liao J, et al. Notch signaling augments BMP9-induced bone formation by promoting the osteogenesis-angiogenesis coupling process in mesenchymal stem cells (MSCs). Cell Physiol Biochem. 2017;41(5):1905–23.
20. Young K, et al. BMP9 regulates endoglin-dependent chemokine responses in endothelial cells. Blood. 2012;120(20):4263–73.
21. Song T, et al. The effect of BMP9 on inflammation in the early stage of pulpitis. J Appl Oral Sci. 2023;31: e20220313.
22. Jiang Q, et al. BMP9 promotes methionine- and choline-deficient diet-induced nonalcoholic steatohepatitis in non-obese mice by enhancing NF-kappaB dependent macrophage polarization. Int Immunopharmacol. 2021;96: 107591.
23. Kusuyama J, et al. Low-intensity pulsed ultrasound promotes bone morphogenic protein 9-induced osteogenesis and suppresses inhibitory effects of inflammatory cytokines on cellular responses via Rho-associated kinase 1 in human periodontal ligament fibroblasts. J Cell Biochem. 2019;120(9):14657–69.
24. Daans M, Lories RJU, Luyten FP. Dynamic activation of bone morphogenetic protein signaling in collagen-induced arthritis supports their role in joint homeostasis and disease. Arthritis Res Ther. 2008;10(5):R115.
25. Verschueren PCPM, et al. Detection, identification and in vivo treatment responsiveness of bone morphogenetic protein (BMP)-activated cell populations in the synovium of patients with rheumatoid arthritis. Ann Rheum Dis. 2009;68(1):117–23.

26. Chemel M, et al. Bone morphogenetic protein 2 and transforming growth factor beta1 inhibit the expression of the proinflammatory cytokine IL-34 in rheumatoid arthritis synovial fibroblasts. Am J Pathol. 2017;187(1):156–62.
27. Song B, et al. BMP9 inhibits the proliferation and migration of fibroblast-like synoviocytes in rheumatoid arthritis via the PI3K/AKT signaling pathway. Int Immunopharmacol. 2019;74: 105685.
28. Brand DD, Latham KA, Rosloniec EF. Collagen-induced arthritis. Nat Protoc. 2007;2(5):1269–75.
29. He, T., Adenoviral vectors. Curr Protoc Hum Genet, 2004. Chapter 12: p. Unit 12.4.
30. Arnett FC, et al. The American Rheumatism Association 1987 revised criteria for the classification of rheumatoid arthritis. Arthritis Rheum. 1988;31(3):315–24.
31. Zhang H, Li H. Tricin enhances osteoblastogenesis through the regulation of Wnt/beta-catenin signaling in human mesenchymal stem cells. Mech Dev. 2018;152:38–43.
32. Zhang Y, et al. Establishment of immortalized rabbit bone marrow mesenchymal stem cells and a preliminary study of their osteogenic differentiation capability. Animal Model Exp Med. 2024;7(6):824–34.
33. Sreekumar V, et al. BMP9 a possible alternative drug for the recently withdrawn BMP7? New perspectives for (re-)implementation by personalized medicine. Arch Toxicol. 2017;91(3):1353–66.
34. Liu L, et al. DLX6-AS1 regulates odonto/osteogenic differentiation in dental pulp cells under the control of BMP9 via the miR-128-3p/MAPK14 axis: a laboratory investigation. Int Endod J. 2024;57(11):1623–38.
35. Zhang J, et al. BMP9 induces osteogenic differentiation through up-regulating LGR4 via the mTORC1/Stat3 pathway in mesenchymal stem cells. Genes Dis. 2024;11(3): 101075.
36. Song T, Huang D, Song D. The potential regulatory role of BMP9 in inflammatory responses. Genes Dis. 2022;9(6):1566–78.
37. Gao X, et al. Impaired bone defect and fracture healing in dystrophin/utrophin double-knockout mice and the mechanism. Am J Transl Res. 2020;12(9):5269–82.
38. Yeremenko N, et al. Tumor necrosis factor and interleukin-6 differentially regulate Dkk-1 in the inflamed arthritic joint. Arthritis Rheumatol. 2015;67(8):2071–5.
39. Liu X, et al. BMP9 overexpressing adipose-derived mesenchymal stem cells promote cartilage repair in osteoarthritis-affected knee joint via the Notch1/Jagged1 signaling pathway. Exp Ther Med. 2018;16(6):4623–31.
40. Wang J, et al. BMP9 and COX-2 form an important regulatory loop in BMP9-induced osteogenic differentiation of mesenchymal stem cells. Bone. 2013;57(1):311–21.
41. Wang H, et al. All-trans retinoic acid and COX-2 cross-talk to regulate BMP9-induced osteogenic differentiation via Wnt/beta-catenin in mesenchymal stem cells. Biomed Pharmacother. 2019;118: 109279.
42. Huang X, et al. Dentinogenesis and tooth-alveolar bone complex defects in BMP9/GDF2 knockout mice. Stem Cells Dev. 2019;28(10):683–94.
43. Kusuyama J, et al. Low-intensity pulsed ultrasound (LIPUS) promotes BMP9-induced osteogenesis and suppresses inflammatory responses in human periodontal ligament-derived stem cells. J Orthop Trauma. 2017;31(7):S4.
44. Wold WSM, Toth K. Adenovirus vectors for gene therapy, vaccination and cancer gene therapy. Curr Gene Ther. 2013;13(6):421–33.

Publisher's Note